第 49 卷 第 23 期/2022 年 12 月/中国激光 研究论文

中国激光

基于环形器的线形腔可控掺镱自扫光纤激光器

左振忠[2,3]，王凯乐[2,3]，黄先明[2,3]，陈浩伟[1,2,3]，陆宝乐[1,2,3**]，白晋涛[1,2,3*]

[1]西北大学省部共建西部能源光子技术国家重点实验室，陕西 西安 710127；

[2]西北大学陕西省全固态激光及应用工程技术研究中心，陕西 西安 710127；

[3]西北大学光子学与光子技术研究所陕西省光电子技术重点实验室，陕西 西安 710127

摘要 展示了一种基于环形器的线形腔可控掺镱自扫光纤激光器，腔两端的反射光在掺镱光纤内形成驻波场，产生空间烧孔效应，进而诱导形成动态光栅，产生自扫效应。当泵浦功率达到 22.5 mW 时，获得了正向自扫效应，当泵浦功率为 48.8 mW 时，获得的最大自扫范围约为 6 nm（1065.4217～1071.4225 nm）。在整个实验过程中，获得的扫描速度为 0.56～8.83 nm/s，平均脉冲重复频率为 12.08～115.20 kHz。当泵浦功率为 161.3 mW 时，获得的最大光学信噪比为 53.18 dB。实验中，在环形器内引入一个机械式可调谐光衰减器，通过改变腔内损耗，简单有效地对自扫范围和自扫速度等自扫特性进行了调控，并将自扫范围扩大为 10.83 nm。

关键词 激光器；光纤激光器；自扫效应；光谱特性；微秒脉冲

中图分类号 O436 **文献标志码** A **DOI**：10.3788/CJL202249.2301003

1 引 言

扫频光纤激光器因其灵活的波长可调谐特性，在光通信、光传感及光谱合成等方面极具应用价值[1-4]，其产生波长可调谐的方法主要依赖于光栅和带通滤波器。为了实现周期性且稳定的波长调谐操作，大多数扫频激光器都采用了电驱动压电陶瓷、加热器或可调谐扫描滤波器等扫描器件[5-8]，这导致激光器的结构变得复杂且输出性能降低，其发展也因此大受影响。近年来，一种基于自扫效应的新型扫频光纤激光器引起了科研人员的广泛关注。相比一般的扫频光纤激光器，自扫光纤激光器的结构简单，可以实现高输出功率和高成本效益，而且无需使用任何复杂的调谐元件和电驱动装置就能实现自发的、稳定的、周期性的波长可调谐。自扫光纤激光器的扫描范围宽（高达 23 nm[9]）且易实现，这使得其在可调谐光源的实际应用中极具吸引力，例如光纤布拉格光栅表征[10]、光谱分析[11]等。其中，瞬时频谱可以包含多个纵模，也可以只有一个纵模，具体取决于腔体参数[12]。在后一种情况下，自扫光纤激光器产生周期性脉冲序列，其中仅包含单纵模辐射。目前大多数文献报道的是 1 μm 掺镱光纤激光器中的自扫效应，但使用其他增益光纤在不同光谱区域同样可以观察到自扫效应：掺钕光纤激光器[13]中的自扫波段大小接近 1.06 μm 及 0.93 μm；掺铋光纤激光器[14]中的自扫波段大小接近 1.46 μm；掺铒光纤激光器[15]中的自扫波段大小接近 1.55 μm；铥-钬共掺[16]、掺钬[17]和掺铥[18-19]光纤激光器中的自扫波段大小接近 2 μm。应该注意的是，在所有的掺杂自扫光纤激光器中，仅掺镱[12]、掺铋[14]、掺铥[19]及掺钕[13]光纤激光器实现了单频宽范围自扫效应。这一事实证明，增益介质的参数，如上能级的寿命或动态光栅中振幅分量和相位分量之间的比率[20]，对自扫效应均存在影响。在首次观察到的自扫效应[21-23]中，激光器的输出波长随时间逐渐增加，并在扫描区域的末端跳回初始位置进入下一个扫描周期，这种扫描方向被定义为正向自扫。在某些条件下，还能实现输出波长随时间逐渐减少的反向自扫，反向自扫效应首次见于 2012 年的掺镱光纤激光器报道中[24]。研究表明，通过改变泵浦功率可以调节扫描状态，在低功率和高功率下分别观察到反向自扫和正向自扫现象[25]。在后续发展中，本课题组分别采用双向环形腔[26-27]以及单向环形腔结构[28]实现了自扫光纤激光器，同时激光器的时域动态从脉冲态发展到了连续波状态。

本文展示了一种基于环形器的线形腔可控掺镱自扫光纤激光器。首先采用环形器替代以往的光纤平切端口作为谐振腔反射镜，实现了正向自扫效应。实验中，在泵浦功率为 22.5～86.3 mW 时，获得的扫描速度范围为 0.56～8.83 nm/s；在泵浦功率为 22.5～

收稿日期：2021-11-15；**修回日期**：2022-01-03；**录用日期**：2022-03-24

基金项目：陕西省重点研发计划国际科技合作项目（2020KW-018）

通信作者：*baijt@nwu.edu.cn；**lubaole1123@163.com

112.5 mW 时，获得的平均脉冲重复频率范围为 12.08～115.20 kHz；实验获得的最大自扫范围约为 6 nm(1065.4217～1071.4225 nm)，最大的光学信噪比为 53.18 dB。之后在环形器内引入一个机械式可调谐光衰减器，通过改变腔内损耗，实现了对激光器自扫范围和自扫速度的灵活调控，并将自扫范围扩大到 10.83 nm。这种自扫调控方式具有操作灵活、简单可靠、成本低廉等优点，可显著改善和提高自扫光纤激光器的运转性能。

2 实验装置和自扫原理

基于环形器的线形腔可控掺镱自扫光纤激光器的实验装置如图 1 所示，其中 VOA 为可调谐光衰减器。采用 975 nm 半导体激光器(LD)为泵浦源，最大输出功率为 650 mW。泵浦光通过 975 nm/1064 nm 的波分复用器(WDM)耦合进入腔内对一段长约 20 cm 的掺镱光纤(YDF)进行泵浦，产生受激放大自发辐射(ASE)光。在 WDM 的信号光端熔接了一个分光比为 50/50 的 2×2 光纤耦合器 1(OC1)，OC1 的两个输出端口被熔接在一起构成光纤环形镜(FLM)，起到全反镜的作用。采用分光比为 20/80 的 1×2 光纤耦合器 2(OC2)的 20%光纤端口作为输出端，将 80%光纤端口连接环形器(CIR)的 2 端口。环形器的 3 端口和 1 端口被熔接在一起构成环状，激光从 CIR 的 2 端口进入，经过 3 端口绕一周后从 1 端口返回进入掺镱光纤进行放大。谐振腔由 FLM 和 CIR 构成，为典型的法布里-珀罗(F-P)线形腔结构。腔内输出端口均采用角度物理接触(APC)光纤跳线熔接，避免不必要的背面反射光干扰自扫效应的正常运行。腔内传输光纤以及各个器件的尾纤均为单模光纤，总腔长约为 4.07 m。

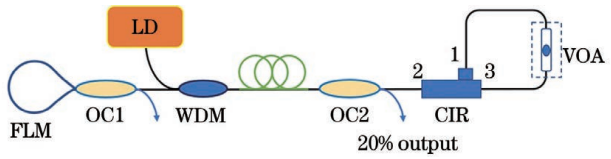

图 1 掺镱自扫光纤激光器实验装置结构图

Fig. 1 Structural diagram of ytterbium-doped self-sweeping fiber laser

实验中采用 CIR 替换光纤平切端口作为谐振腔的一端，光纤平切端口能够提供 3.5%(能量占比)的菲涅耳反射光，其余 96.5%(能量占比)的激光都被透射出腔外，导致损耗很大，使得激光器的起振阈值变得很高。虽然使用 CIR 也存在一定插入损耗，但相比光纤平切端口，其能够大大降低激光器阈值。自扫效应的产生归因于谐振腔内的激光在有源光纤内形成的驻波场，驻波场产生的空间烧孔(SHB)效应[22]引起光强的空间周期性分布，粒子数反转会引起有源光纤折射率的变化，即在驻波波节处增益大，波腹处增益小。因此，沿着有源光纤会诱导出类似于分布式光栅的结构，即“增益光栅”。通过调控谐振腔内的损耗，有源介质中的增益特性[29](例如增益饱和、弛豫振荡等)会发生改变，即增益曲线轮廓及增益光栅的周期性特性发生动态改变，进而参与自扫过程的激光纵模的频率大小及数目发生改变，最终表现出激光输出的扫描范围和扫描速率发生变化。

3 实验结果与讨论

3.1 自扫效应的光谱特性研究

在自扫光纤激光器中，自扫效应一般不会出现在激光阈值处，而是在高于激光器阈值的某个功率范围内产生并持续运作一段时间。这是由于形成自扫的稳定条件被腔内的受激布里渊散射(SBS)效应、受激拉曼散射(SRS)效应等非线性效应破坏。本实验中自扫光纤激光器的起振阈值为 20.3 mW，自扫阈值为 22.5 mW，其明显特征体现在输出光谱动态上，采用分辨率为 0.034 nm@1 μm 的光谱分析仪(OSA)观测输出波长的波动。当泵浦功率为 48.8 mW 时，自扫光纤激光器的输出光谱如图 2 所示。图 2(a)显示激光器的中心输出波长从 1065.4217 nm 漂移到 1071.4225 nm，每个输出光谱都是 OSA 在不同时刻下单次记录获得的，波长扫描范围约为 6 nm。从图 2(a)可以看出，该激光器产生的是正向自扫，输出的各个中心波长对应的功率基本相似，稳定性较好。由于我们使用的 OSA 不具备很快的扫描速度，最小采集速度仅为 1 s 采一个点，即使调节OSA的扫描范

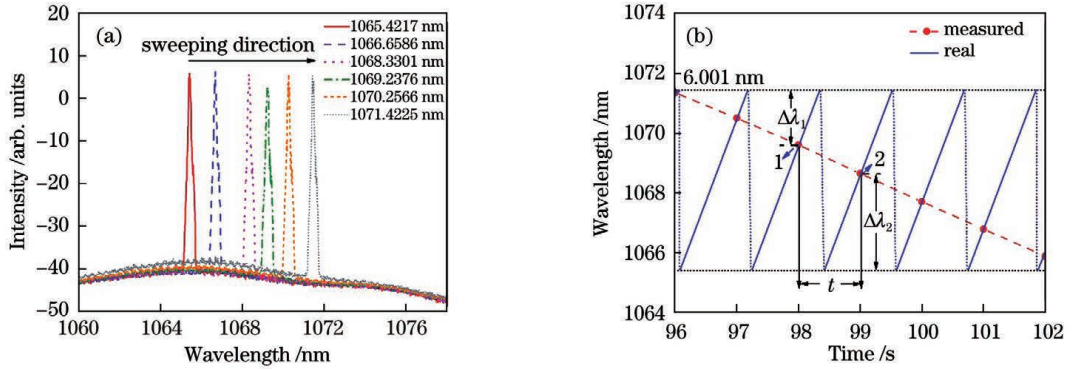

图 2 泵浦功率为 48.8 mW 时自扫激光器的输出光谱动态图。(a)光谱序列；(b)输出频谱

Fig. 2 Dynamic output spectra of self-sweeping laser with pump power of 48.8 mW. (a) Spectral sequence; (b) output spectra

围也无法分析本实验的自扫现象，这导致实验中不能直接观测到激光器的实际激光线扫描，需要进行具体分析，分析方法类似于文献[15]。如图 2(b)所示，虚线为 OSA 上观测记录的激光线扫描，实线为我们通过数据具体分析后得到的激光器真正的激光线扫描。

其中，在 t 时间范围内，具体的运行轨迹为点 1 处的中心波长移动到扫描波长最大值处，再瞬间跳回到扫描波长最小值处，之后再漂移到点 2 中心波长处，因此可以对自扫速度进行推算[15]：

$$\nu=\frac{\Delta\lambda_1+\Delta\lambda_2}{t}, \tag{1}$$

式中：ν 为自扫速度，单位为 nm/s；t 为两个中心波长值的时间间隔，大小为 1 s；$\Delta\lambda_1$ 为点 1 处的中心波长值与扫描能达到的波长最大值的差值；$\Delta\lambda_2$ 为点 2 处的中心波长值与扫描能达到的波长最小值的差值；$\Delta\lambda_1+\Delta\lambda_2$ 为 1 s 时间内中心波长的漂移总长度，单位为 nm。通过计算可知扫描速度为 5.213 nm/s。

3.2 自扫效应的脉冲时域动态

采用数字存储示波器测量了自扫光纤激光器输出的时域强度动态，如图 3 所示。图 3(a)显示了激光器输出的是宽度为微秒量级的短脉冲序列，即激光器在自脉冲状态下工作。图 3(b)显示微秒脉冲以模间拍频[22]方式进行调制：

$$\Delta\nu=\frac{c}{2nL}, \tag{2}$$

式中：c 为真空中的光速（$\sim3\times10^8$ m/s）；n 为有效折射率（~1.47）；$\Delta\nu$ 为纵模拍频间隔（~25 MHz）；L 为激光器腔长。通过计算可得腔长约为 4.08 m，与实际测量值吻合。在我们实验中，自扫效应的出现往往伴随着自脉冲现象，而自脉冲是由弛豫振荡引起的，其平均脉冲重复频率 ΔV 由腔中光子寿命 τ 和泵浦功率 P_p 或者输出功率 P_{out} 和腔长 L 决定[30]：

$$\Delta V^2\propto\frac{1}{\tau}\left(\frac{P_p}{P_{th}}-1\right)\propto\frac{P_{out}}{L}, \tag{3}$$

式中：P_{th} 为激光器阈值功率。

根据弛豫振荡理论，在腔长 L 确定的条件下，随着输出功率 P_{out} 的增大，短脉冲序列的时间间隔减小，平均脉冲重复频率 ΔV 增大。

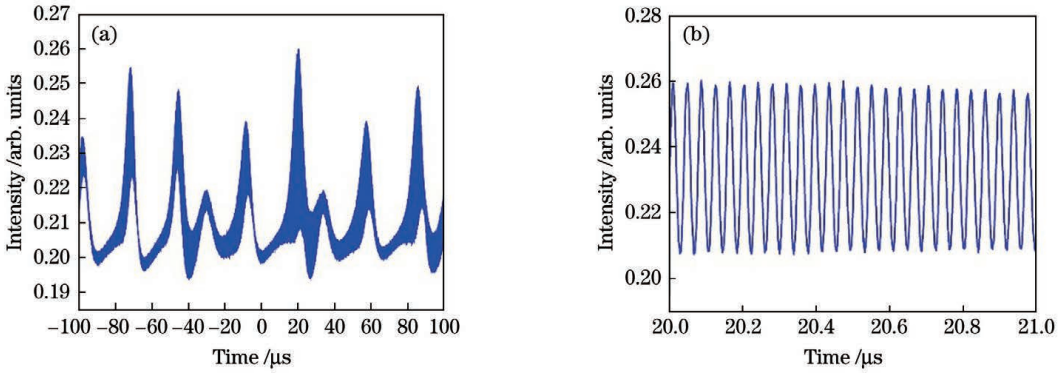

图 3 泵浦功率 37.5 mW 时激光器的脉冲信号。(a)微秒脉冲动态；(b)单个脉冲放大后的纵向拍频细节

Fig. 3 Pulse signal of laser at pump power of 37.5 mW. (a) Microsecond pulse dynamics; (b) detail of longitudinal beat after amplification of single pulse

3.3 自扫效应的规律特性研究

采用功率计对自扫光纤激光器的输出功率斜率效率进行测量。在该激光器泵浦功率由 22.5 mW 增加到 157.5 mW 的情况下，输出功率随泵浦功率的增大线性增加，斜率效率约为 10.65%，如图 4(a)所示。如图 4(b)所示，随着输出功率的增加，自扫范围会逐渐增加。增益光纤的增益轮廓随着泵浦功率的增加而升高，导致出现更宽的激光光谱范围，因此会有更多不同频率的纵模模式参与激光器的自扫产生过程，从而产生 SHB 效应，进而激光器的中心输出波长可以在更宽范围内扫描；当扫描范围达到最大值之后，受到腔内 SBS 效应、SRS 效应等非线性效应的干扰，自扫范围会逐渐减小直至慢慢消失，最大扫描范围约为 6 nm，这可能是我们所使用的增益介质太短（~20 cm）导致的[9]。实验中，如图 4(c)、(d)所示，随着输出功率的增加，平均脉冲重复频率从 12.08 kHz 增加至 115.2 kHz，扫描速度由 0.56 nm/s 逐渐增大至 8.83 nm/s。其中，自扫速度和平均脉冲重复频率与输出功率的函数关系存在一致性，即二者都会随着输出功率的增加而增加，与输出功率的平方呈线性比例关系。

3.4 激光器的光学信噪比

由图 2(a)可知，实现的自扫光纤激光器在泵浦功率不高的情况下输出光谱的光学信噪比（OSNR）均高于 40 dB。当泵浦功率逐渐增加时，OSNR 也会逐渐增大。图 5(a)显示，当泵浦功率为 86.3 mW 时，输出中心波长为 1067.1503 nm 处的光学信噪比高达 51.42 dB。当泵浦功率增加至 161.3 mW 时，OSNR 会达到最大值 53.18 dB，如图 5(b)所示，此时输出中心波长位于 1070.7140 nm。通常 OSNR 越大，光信号受噪声的干扰越小，有效功率越高。因此实现的自扫光纤激光器的输出性能优良。

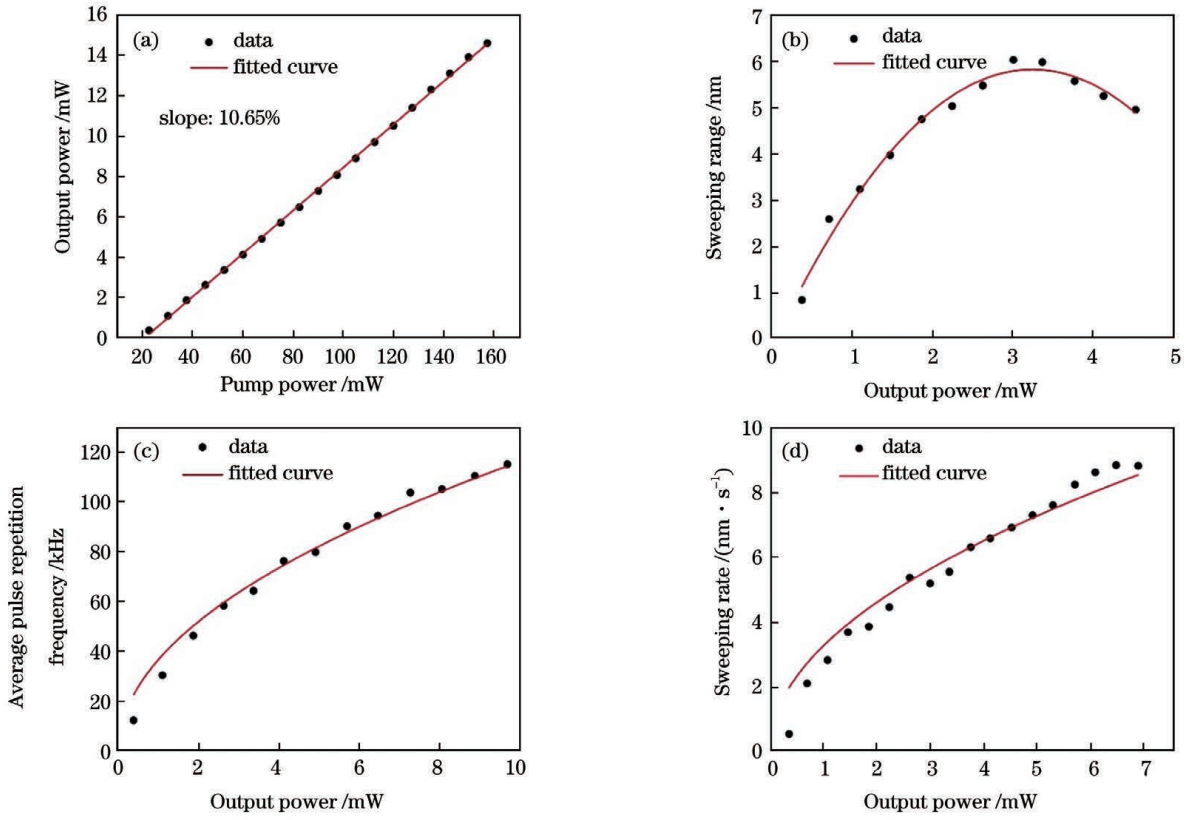

图 4 光纤激光器的输出特性。(a)输出功率随泵浦功率的变化；(b)扫描范围随输出功率的变化；(c)平均脉冲重复频率随输出功率的变化；(d)扫描速率随输出功率的变化

Fig. 4 Output characteristics of fiber laser. (a) Output power versus pump power; (b) sweeping range versus output power; (c) average pulse repetition frequency versus output power; (d) sweeping rate versus output power

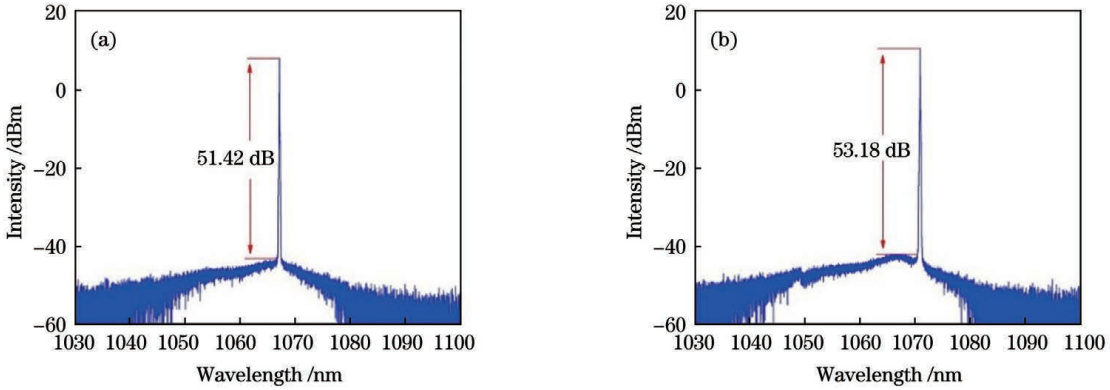

图 5 不同泵浦功率下输出光谱的 OSNR。(a)86.3 mW；(b)161.3 mW

Fig. 5 OSNRs of output spectra under different pump powers. (a) 86.3 mW; (b) 161.3 mW

3.5 通过改变腔损耗来调控自扫范围和自扫速度

由图 4(b)、(d)可知，自扫范围和自扫速度对输出功率有一定的依赖关系，因此可以通过调节腔内损耗来改变激光器的输出功率，从而实现自扫范围和自扫速度的调控。在实验装置(图 1)中，在 CIR 的 1 端口和 3 端口之间引入一个机械式可调谐光衰减器，以此实现腔内损耗的连续调谐变化，如图 1 中虚线框部分所示。当泵浦功率为 52.5 mW 时，通过调节 VOA 实现腔内损耗增加，这个过程中的自扫激光光谱如图 6 所示。由图 6(a1)、(a2)看出，当激光器中心输出波长从 1062.3791 nm 漂移到 1067.4092 nm 时，扫描范围为 5.031 nm，扫描速度为 5.346 nm/s；由图 6(b1)、(b2)看出，当自扫范围在 1060.4860～1065.1042 nm 区间时，扫描范围为 4.618 nm，扫描速度为 3.658 nm/s；由图 6(c1)、(c2)看出，光纤激光器的扫描范围为 3.691 nm(1056.5773～1060.2672 nm)，扫描速度为 2.838 nm/s。实验结果表明，随着腔内损耗的增加，自扫波段范围逐渐向短波长方向漂移，自扫速度逐渐变慢，自扫范围逐渐变窄，但扫描范围扩大到 10.83 nm(1056.5773～1067.4093 nm)。因此通过 VOA 连续改变谐振腔损耗是一种行之有效的实现自扫光纤激光器灵活调控输出的技术手段。

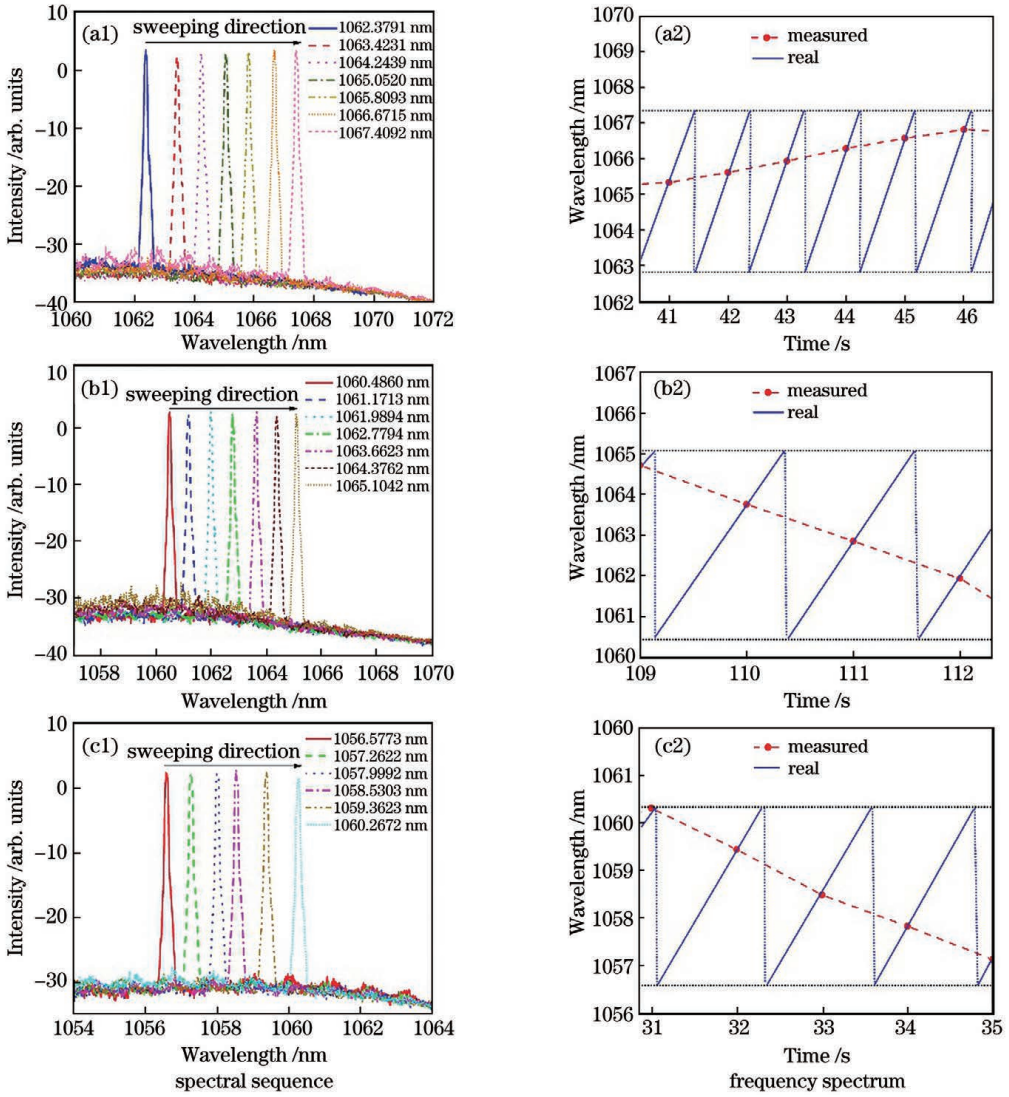

图 6　泵浦功率为 52.5 mW 时通过调节 VOA 实现的三种自扫激光光谱。(a1)(a2)扫描范围为 5.031 nm;(b1)(b2)扫描范围为 4.618 nm;(c1)(c2)扫描范围为 3.691 nm

Fig. 6　Three self-sweeping spectra realized by adjusting VOA at 52.5 mW pump power. (a1) (a2) Scanning range is 5.031 nm; (b1)(b2) scanning range is 4.618 nm; (c1)(c2) scanning range is 3.691 nm

4　结　　论

通过使用 CIR 替代光纤平切端口作为谐振腔反射端，实现了产生正向自扫效应的线形腔掺镱自扫光纤激光器，获得了约 6 nm 的扫描范围、0.56～8.83 nm/s 的扫描速度和 12.08～115.2 kHz 的平均脉冲重复频率。激光器输出光谱的 OSNR 均大于 40 dB，最大时可达 53.18 dB，这表明输出性能良好。当在 CIR 内引入一个机械式 VOA 时，通过调节 VOA 来改变腔内损耗，可以实现自扫范围和自扫速度等自扫特性的调控，并将扫描范围扩大至 10.83 nm。提供了一种简单有效、稳定以及低成本的自扫调控方式，该方法有助于促进自扫光纤激光器在光谱测量、分析等激光领域中的实际应用。

参　考　文　献

[1]　Ryu C Y, Hong C S. Development of fiber Bragg grating sensor system using wavelength-swept fiber laser[J]. Smart Materials and Structures, 2002, 11(3): 468-473.

[2]　Wei F, Lu B, Wang J, et al. Precision and broadband frequency swept laser source based on high-order modulation-sideband injection-locking[J]. Optics Express, 2015, 23(4): 4970-4980.

[3]　Gotti R, Puppe T, Mayzlin Y, et al. Comb-locked frequency-swept synthesizer for high precision broadband spectroscopy[J]. Scientific Reports, 2020, 10: 2523.

[4]　梅佳伟，肖晓晟，许明睿，等. 基于色散调谐宽带扫频光纤激光器及其在光纤光栅解调中的应用[J]. 光学学报, 2012, 32(11): 1114003.
Mei J W, Xiao X S, Xu M R, et al. Wavelength-swept fiber laser based on dispersion tuning and its application on the demodulation of fiber bragg grating[J]. Acta Optica Sinica, 2012, 32(11): 1114003.

[5]　陆龙钊，张大鹏，曾厚财，等. 基于短环形腔制备高速扫频光源的研究[J]. 光学学报, 2020, 40(24): 2414001.
Lu L Z, Zhang D P, Zeng H C, et al. Study on the fabrication of high-speed swept source based on short ring cavity[J]. Acta Optica Sinica, 2020, 40(24): 2414001.

[6]　邢志坤，宋青果，牟成博，等. 基于 45°倾斜光纤光栅辐射模的线偏振调谐光纤激光器[J]. 中国激光, 2020, 47(12): 1201007.

Xing Z K, Song Q G, Mou C B, et al. Linear polarized tunable fiber laser based on radiation mode of 45°-tilted fiber grating[J]. Chinese Journal of Lasers, 2020, 47(12): 1201007.
[7] 韦达, 冯亭, 延凤平, 等. 傅里叶域锁模扫频光纤激光器研究方法: 以掺铒光纤激光器为例[J]. 中国激光, 2021, 48(16): 1601003.
Wei D, Feng T, Yan F P, et al. Frequency-swept fiber laser based on Fourier-domain mode-locking: a case study on erbium-doped fiber laser[J]. Chinese Journal of Lasers, 2021, 48(16): 1601003.
[8] 李国玉, 杨康, 贾素梅, 等. 基于压电陶瓷闭环控制的线性可调谐环形腔光纤激光器[J]. 光学学报, 2015, 35(6): 0614003.
Li G Y, Yang K, Jia S M, et al. Linear tunable fiber ring laser based on closed-loop piezoelectric ceramics[J]. Acta Optica Sinica, 2015, 35(6): 0614003.
[9] Lobach I A, Tkachenko A Y, Kablukov S I. Optimization and control of the sweeping range in an Yb-doped self-sweeping fiber laser[J]. Laser Physics Letters, 2016, 13(4): 045104.
[10] Lobach I A, Kablukov S I. Application of a self-sweeping Yb-doped fiber laser for high-resolution characterization of phase-shifted FBGs[J]. Journal of Lightwave Technology, 2013, 31(18): 2982-2987.
[11] Tkachenko A Y, Lobach I A, Kablukov S I. All-fiber Brillouin optical spectrum analyzer based on self-sweeping fiber laser[J]. Optics Express, 2017, 25(15): 17600-17605.
[12] Lobach I A, Kablukov S I, Podivilov E V, et al. Self-scanned single-frequency operation of a fiber laser driven by a self-induced phase grating[J]. Laser Physics Letters, 2014, 11(4): 045103.
[13] Kashirina E K, Lobach I A, Kablukov S I. Single-frequency self-sweeping Nd-doped fiber laser[J]. Optics Letters, 2019, 44(9): 2252-2255.
[14] Lobach I A, Kablukov S I, Melkumov M A, et al. Single-frequency Bismuth-doped fiber laser with quasi-continuous self-sweeping[J]. Optics Express, 2015, 23(19): 24833-24842.
[15] Navratil P, Peterka P, Vojtisek P, et al. Self-swept erbium fiber laser around 1.56 μm[J]. Opto-Electronics Review, 2018, 26(1): 29-34.
[16] Wang X, Zhou P, Wang X L, et al. Tm-Ho co-doped all-fiber brand-range self-sweeping laser around 1.9 μm[J]. Optics Express, 2013, 21(14): 16290-16295.
[17] Aubrecht J, Peterka P, Koška P, et al. Self-swept holmium fiber laser near 2100 nm[J]. Optics Express, 2017, 25(4): 4120-4125.
[18] Budarnykh A E, Vladimirskaya A D, Lobach I A, et al. Broad-range self-sweeping single-frequency linearly polarized Tm-doped fiber laser[J]. Optics Letters, 2018, 43(21): 5307-5310.
[19] Jiang H B, Lei J, Set S Y, et al. Spontaneous laser line sweeping in Tm doped fiber laser[C]//Laser Congress 2018 (ASSL), November 4-8, 2018, Boston, Massachusetts. Washington, D.C.: OSA, 2018: AM6A.34.
[20] Stepanov S. Dynamic population gratings in rare-earth-doped optical fibres[J]. Journal of Physics D: Applied Physics, 2008, 41(22): 224002.
[21] Kir'yanov A V, Il'ichev N N. Self-induced laser line sweeping in an ytterbium fiber laser with non-resonant Fabry-Perot cavity[J]. Laser Physics Letters, 2011, 8(4): 305-312.
[22] Lobach I A, Kablukov S I, Podivilov E V, et al. Broad-range self-sweeping of a narrow-line self-pulsing Yb-doped fiber laser[J]. Optics Express, 2011, 19(18): 17632-17640.
[23] Peterka P, Navrátil P, Maria J, et al. Self-induced laser line sweeping in double-clad Yb-doped fiber-ring lasers[J]. Laser Physics Letters, 2012, 9(6): 445-450.
[24] Peterka P, Navratil P, Dussardier B, et al. Self-induced laser line sweeping and self-pulsing in double-clad fiber lasers in Fabry-Perot and unidirectional ring cavities[J]. Proceedings of SPIE, 2012, 8433: 843309.
[25] Navratil P, Peterka P, Honzatko P, et al. Reverse spontaneous laser line sweeping in ytterbium fiber laser[J]. Laser Physics Letters, 2017, 14(3): 035102.
[26] Wang K L, Wen Z R, Chen H W, et al. Observation of reverse self-sweeping effect in an all-polarization-maintaining bidirectional ytterbium-doped fiber laser[J]. Optics Express, 2020, 28(9): 13913-13920.
[27] Wang K L, Wen Z R, Chen H W, et al. Wavelength-flexible all-polarization-maintaining self-sweeping fiber laser based on intracavity loss tuning[J]. Chinese Optics Letters, 2021, 19(4): 041401.
[28] Wen Z R, Wang K L, Chen H W, et al. Self-sweeping ytterbium-doped fiber laser based on a fiber saturable absorber[J]. Applied Physics Express, 2021, 14(1): 012005.
[29] 彭昭亮, 马善超, 陆思华, 等. 增益调制掺铥光纤激光器的数值仿真及实验研究[J]. 激光与光电子学进展, 2020, 57(19): 191404.
Peng Z L, Ma S C, Lu S H, et al. Numerical simulation and experimental study of gain-switched thulium-doped fiber laser[J]. Laser & Optoelectronics Progress, 2020, 57(19): 191404.
[30] Orsila L, Okhotnikov O. Three- and four-level transition dynamics in Yb-fiber laser[J]. Optics Express, 2005, 13(9): 3218-3223.

Linear-Cavity-Controlled Self-Sweeping Ytterbium-Doped Fiber Laser Based on Circulator

Zuo Zhenzhong[2,3], Wang Kaile[2,3], Huang Xianming[2,3], Chen Haowei[1,2,3], Lu Baole[1,2,3**], Bai Jintao[1,2,3*]

[1] *State Key Laboratory of Photon-Technology in Western China Energy, Northwest University, Xi'an* 710127, *Shaanxi, China*;
[2] *Shaanxi Engineering Technology Research Center for Solid State Lasers and Application, Northwest University, Xi'an* 710127, *Shaanxi, China*;
[3] *Provincial Key Laboratory of Photo-Electronic Technology, Institute of Photonics and Photon-Technology, Northwest University, Xi'an* 710127, *Shaanxi, China*

Abstract

Objective Due to the rapid development of fiber laser technology, tunable fiber lasers have become an important development direction of fiber lasers. Their flexible wavelength tuning characteristics are highly valuable in optical communication, optical sensing, and spectral synthesis. However, to achieve a periodic and stable wavelength tuning

operation, tunable fiber lasers often use electrically driven piezoelectric ceramics, heaters, fiber gratings or tunable sweeping filters, and other sweeping devices, which results in a complex structure and reduced output performance of the fiber laser, significantly limiting its development and practical applications.

In recent years, a new type of tunable fiber laser based on the self-sweeping effect has gained the interest of researchers. Compared with general tunable fiber lasers, the self-sweeping fiber laser can achieve spontaneous, stable, and periodic wavelength tunability without using complex tuning elements or electrically driven drives. The phenomenon of the self-sweeping effect was first reported in 1962 when a periodic shift of wavelength was observed in a ruby laser. Half a century later, based on the excellent waveguide medium of optical fiber, researchers in Russia realized the first ytterbium-doped (Yb-doped) self-sweeping fiber laser. Thereafter, based on the typical Fabry–Perot linear cavity structure, researchers observed the self-scanning effect in different bands using different gain media. These bands have greatly facilitated the application of self-sweeping fiber lasers in various research fields and self-sweeping fiber lasers have become one of the research hotspots. In this study, we design a linear-cavity–controlled Yb-doped self-sweeping fiber laser based on a circulator, which is easy to implement, inexpensive, and flexible in controlling the self-sweeping characteristics, such as self-sweeping range and self-sweeping rate, potentially expanding the practical applications of self-sweeping fiber lasers.

Methods In this study, a Yb-doped self-sweeping fiber laser based on a circulator is built based on the previous Fabry–Perot linear cavity structure using a circulator instead of a flat-cut port of the fiber as the reflecting end of the resonant cavity. The resonant cavity of the laser consists of a fiber loop mirror and a circulator. The 3-port and 1-port of the circulator are fused together to form a ring. The laser enters from the 2-port, passes through the 3-port, and returns to the Yb-doped fiber for amplification from the 1-port. The flat-cut port of the fiber can provide 3.5% energy of the Fresnel reflected light, whereas the remaining 96.5% energy of the laser is transmitted out of the cavity, resulting in large losses and a high self-sweeping threshold. Although the circulator has some insertion loss, it can significantly reduce the self-sweeping threshold compared with the fiber flat-cut port. Additionally, since the self-sweeping range and self-sweeping rate are dependent on the output power, the output power of the laser can be changed to regulate the self-sweeping range and self-sweeping rate by adjusting the intracavity loss. By introducing a mechanically variable optical attenuator in the circulator, the self-sweep range and self-sweep speed of the laser can be adjusted flexibly by changing the intracavity loss.

Results and Discussions When the laser is operated with self-sweeping mode, its self-sweeping threshold is only 22.5 mW, the output slope efficiency is 10.65%, and a self-sweeping range of 1065.4217–1071.4225 nm (approximately 6 nm) and a self-sweeping rate of 0.56–8.83 nm/s are obtained, which can be observed in the range of 12.08–115.2 kHz (Fig. 4). The optical signal-to-noise ratios (OSNRs) of the laser output spectra are all greater than 40 dB, with a maximum value of 53.18 dB, indicating a good output performance (Fig. 5). A summary of the characteristics of the self-sweeping law reveals that the self-sweeping rate and average pulse repetition frequency are consistent as a function of the output power, i.e., both increase with the increase of output power and are linearly proportional to the square of the output power. After the introduction of a mechanically variable optical attenuator, the experimental results obtained by adjusting the optical attenuator to change the intracavity loss show that with the increase of intracavity loss, the self-sweeping band range gradually drifts toward the short wavelength direction, the self-sweeping rate gradually becomes slower, and the self-sweeping range gradually becomes narrower. The sweeping range in the whole process can cover 1056.5773–1067.4093 nm, approximately 10.83 nm (Fig. 6). Therefore, using a variable optical attenuator to continuously change the resonant cavity loss is an effective technical method for achieving flexible output control of the self-sweeping fiber laser.

Conclusions In this study, a linear cavity Yb-doped self-sweeping fiber laser that produces a normal self-sweeping effect is realized using a circulator as the reflecting end of the resonant cavity rather than a flat-cut port of the fiber. The cavity structure is simple, easy to implement, and inexpensive. The self-sweeping threshold of the laser is only 22.5 mW, the output slope efficiency is 10.65%, and a self-sweeping range of 1065.4217–1071.4225 nm (approximately 6 nm) and a self-sweeping rate of 0.56–8.83 nm/s with an average pulse repetition frequency of 12.08–115.2 kHz are obtained. The OSNRs of the laser output spectra are all greater than 40 dB, with a maximum of 53.18 dB, which indicates good output performance. When a mechanically variable optical attenuator is introduced into the circulator, the self-sweeping characteristics, such as self-sweeping range and self-sweeping rate, can be adjusted by adjusting the variable optical attenuator to change the cavity loss and extend the sweeping range to 10.83 nm. Our experiments provide a simple, effective, stable, and low-cost method for self-sweeping modulation, potentially facilitating the practical application of self-sweeping fiber lasers in spectral measurement, analysis, and other laser applications.

Key words lasers; fiber lasers; self-sweeping effect; spectral characteristics; microsecond pulse